

Supporting Information

Sterically Controlled Azomethine Ylide Cycloaddition Polymerization of Phenyl-C₆₁-butyric Acid Methyl Ester

Meera Stephen,^{1,2} Hasina H. Ramanitra,¹ Hugo Santos Silva,¹ Simon Dowland,⁴ Didier Bégué,³ Kristijonas Genevičius,² Kestutis Arlauskas,² Gytis Juška,² Graham Morse,⁵ Andreas Distler,⁴ Roger C. Hiorns^{6*}

- 1 Université de Pau et des Pays de l'Adour (UPPA), IPREM (EPCP, CNRS-UMR 5254), 2 Avenue Président Angot, 64053 Pau, France.
- 2 Department of Solid State Electronics, Vilnius University, Lithuania.
- 3 Université de Pau et des Pays de l'Adour (UPPA), IPREM (ECP, CNRS-UMR 5254), 2 Avenue Président Angot, 64053 Pau, France.
- 4 Belectric OPV GmbH, Landgrabenstr. 94, 90443 Nürnberg, Germany.
- 5 Merck Chemicals Ltd., Chilworth Technical Centre, University Parkway, SO16 7QD, Southampton, United Kingdom.
- 6 CNRS, IPREM (EPCP, CNRS-UMR 5254), 64053 Pau, France.

E-mail: roger.hiorns@univ-pau.fr

Contents

Experimental details

	Chemicals
	Equipment and Software
	Device Preparation
	Photo-CELIV
Scheme S1.	Proposed general SACAP reaction scheme with PCBM
Figure S1.	¹ H NMR (CDCl ₃ , ambient temperature) of PPCBMB
Figure S2.	¹³ C NMR (CDCl ₃) of PPCBMB
Figure S3.	DOSY 2-D ¹ H NMR (C ₆ D ₆ , ambient temperature) of PPCBMB
Figure S4.	LUMO frontier orbitals for PCBM
Figure S5.	LUMO frontier orbitals for PCBM-1
Table S1.	Energetic values calculated for C ₆₀ , PCBM, and the most probable structures PCBM-1 and PCBM-2
Table S2.	Calculated reorganization energies
Figure S6.	Cyclic voltammograms of PCBM and PPCBMB.
Figure S7.	Normalized UV-visible absorption spectra of PCBM, PPCBMB and 2,5-bis(octyloxy)terephthalaldehyde
Figure S8.	TGA of PPCBMB (N ₂ , 10 °C min ⁻¹)
Figure S9.	DSC thermogram of the second cycle heating (10 °C min ⁻¹)
Figure S10.	Images of PPCBMB and PPCBMB thin film on ITO substrate
Figure S11.	Photo-CELIV transients and mobility values for P3HT:PPCBMB based devices

Chemicals

All starting materials, except for PCBM (PV-A600) from Merck KGaA (Germany), were purchased from Sigma-Aldrich (France) in their analytical grades and used as received. Toluene and THF were distilled from their respective drying agents, i.e., sodium or sodium and benzophenone, under dry nitrogen. 1,2-Dichlorobenzene (DCB) was degassed under reduced pressure and nitrogen-flushed prior to use. Polymerizations were performed in flame-dried, dry-nitrogen flushed Schlenk vessels under cover from light.

Equipment and Software

^1H (400.6 MHz), ^{13}C (100.16 MHz), and 2-D NMRs were recorded on a Bruker® Avance 400 spectrometer at ambient temperature using solvents as indicated. Characterisations using size exclusion chromatography (SEC) were performed either: at 30 °C with THF as eluent at a flow rate of 1 mL min⁻¹, a toluene flow marker, a bank of 4 columns (Shodex KF801, 802.5, 804, and 806) each of length 300 mm and diameter 8, the whole controlled by Malvern pump (Viskotek, VE1122) connected to Malvern VE3580 refractive index and VE3210 UV-visible detectors; or at 50 °C with HPLC grade chlorobenzene as eluent at a flow rate of 1 mL min⁻¹ through a PLgel 10 µm Mixed-B (300 × 7.5 mm) SEC column controlled by an Agilent Technologies 1260 system and characterised with a refractive index detector. Calibration was against polystyrene standards and samples (0.5 to 4 mg mL⁻¹) were pre-filtered. UV-visible spectra were recorded on a Shimadzu UV-2450PC spectrophotometer.

Thermogravimetric analyses (TGA) were performed on a TA Instruments TGA Q50 at a heating rate of 10 °C min⁻¹ under nitrogen. Differential scanning calorimetry was performed on a Perkin Elmer DSC8000 with solid samples in aluminium crucibles at a heating/cooling rate of 10 °C min⁻¹ under a flux of N₂ maintained at 20 mL min⁻¹. Data treatment was performed with a Pyris™ series DSC8000 software.

Cyclic voltammetry studies were carried out using a three-electrode assembly cell from Bio-Logic SAS and a micro-AUTOLAB Type III potentiostat-galvanostat. Measurements were performed using a glassy carbon electrode in 1,2-dichlorobenzene/acetonitrile (4:1 v/v) solutions containing 0.1 M tetrabutylammonium hexafluorophosphate as electrolyte, Ag/AgNO₃ as the reference electrode, and a platinum-wire counter electrode at a scan rate 50 mV s⁻¹. The final results were

calibrated with the ferrocene/ferrocenium (Fc/Fc⁺) couple. The LUMO of PCBM and PPCBMB were calculated assuming the ferrocene/ferrocenium energy level to be 4.8 eV below the vacuum level,^{S1} such that:

$$E_{\text{LUMO}} = -(E_{1/2} + 4.8) \text{ eV}$$

All DFT calculations employed the RIJCOSX approximation run in Orca 3.0.3 software.^{S2}

Device preparation

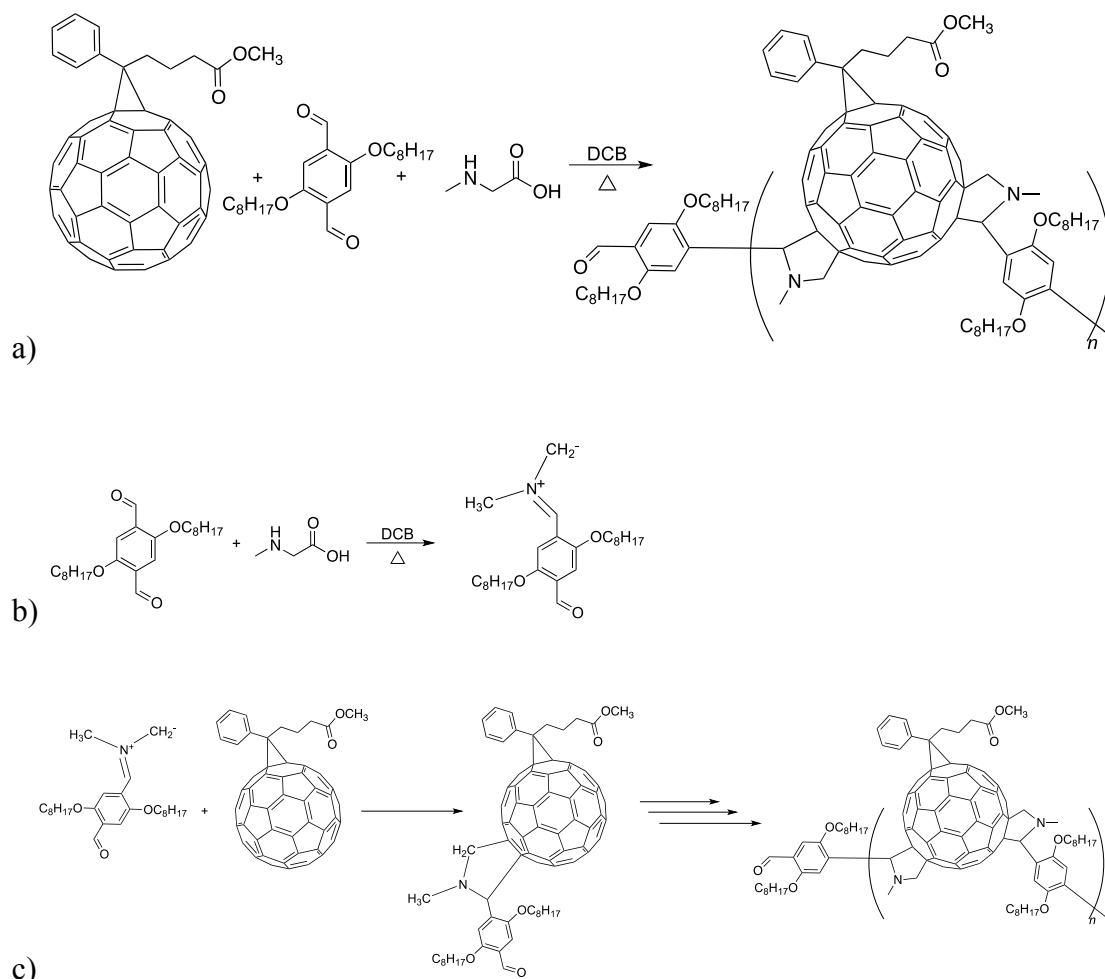
ITO/glass substrates were cleaned by sonication in acetone and isopropyl alcohol. ZnO was coated onto the clean substrates from a nanoparticle suspension (5 wt% in ethanol) and annealed at 140 °C in air. An initial solution of PPCBMB in *o*-xylene was prepared at 12 mg ml⁻¹ by stirring at 80 °C overnight under air. The active layer was coated from a blend solution containing (1:0.8) ratio of P3HT:PPCBMB at a concentration of 27 mg ml⁻¹ in *o*-xylene, followed by a layer of PEDOT:PSS (Heraeus) and subsequent annealing in nitrogen at 140 °C for 5 min. All aforementioned depositions were carried out with a doctor blade. The devices were completed by thermal evaporation of silver under high vacuum to produce cells with 27 mm² active area. The current voltage characteristics were measured under N₂ using a Keithley 2400 source meter and a Xenon arc lamp with an intensity of approximately 100 mWcm⁻².

Photo-CELIV

Photo-CELIV measurements were carried out on the devices prepared as detailed above. The sample was illuminated by a 0.1 mJ laser pulsed at 3-5 ns (EKSPLA-NT 340). Triangular pulses with a rise speed of $2 \times 10^4 \text{ V s}^{-1}$ were applied using a function generator (Tektronix AFG 3011) and current transients were recorded using an oscilloscope (Tektronix DPO 4054B) with 50 Ω input impedance. Variable delay times (t_{del}) were controlled by the function generator. The drift mobility in the case of volume photogeneration under conditions where the capacitive displacement current j_0 remains comparable to the conductivity current (Δj), was calculated using the equation:

$$\mu = \frac{2d^2}{3At_{\text{max}}^2(1 + 0.36\Delta j/j_0)}$$

where t_{max} corresponds to the maximum of the current transient, d is the thickness of active layer, and A is the rise speed of the applied voltage pulse.^{S3}



Scheme S1. Proposed general SACAP reaction scheme with PCBM. Above (a) the overall reaction showing the most probable regioisomers in accordance with the calculated electronic LUMO densities and steric considerations (*vide infra*). The fullerene cycloadditions occur at [6,6]-bonds, however, there are 30 of these around the sphere, so it is more than probable that a number of regioisomers exist in the chain. It is thought that in SACAP, the reaction is such that the fullerene moiety of the PCBM undergoes two additions with azomethine ylides thereby forming a polymer. Tertiary additions are reduced by employing sterically cumbersome comonomers. Below (b) the initial steps based on the Prato reaction,^{S4} in which the aldehyde reacts with sarcosine to form the azomethine ylide *in situ*, which then reacts in a concerted fashion with the fullerene [6,6]-double bond to form the pyrrolidine ring. The SACAP reaction is thought to continue as a polyaddition as shown in (c).

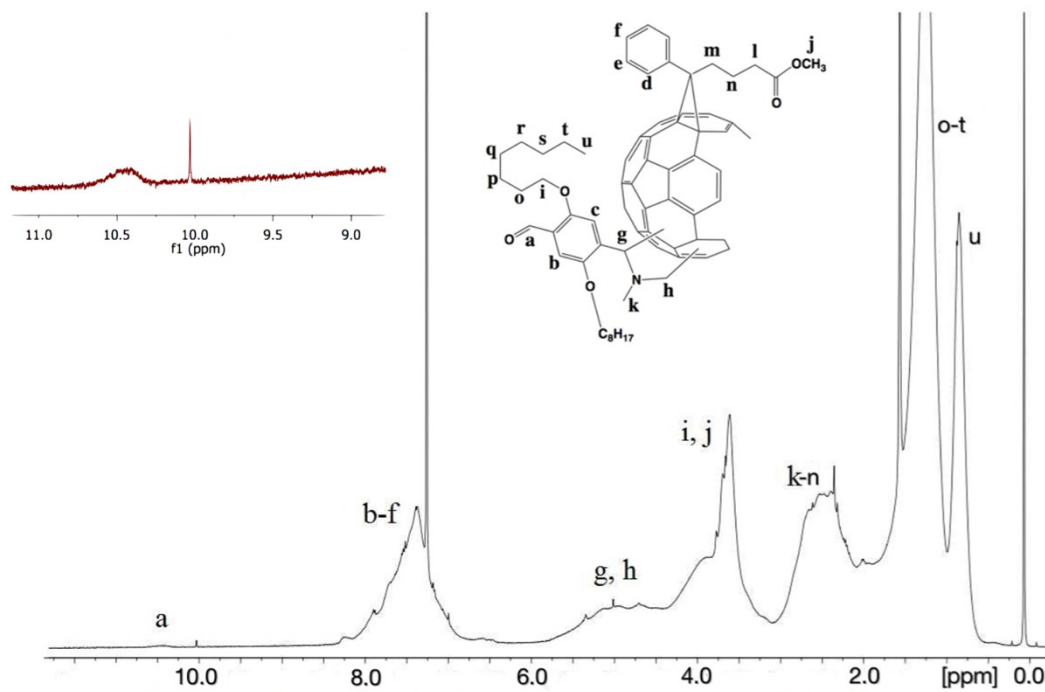


Figure S1. ¹H NMR (CDCl₃, ambient temperature) of PPCBMB, with the inset showing aldehyde region enlarged. Note peaks due to grease (0.01 ppm), water (1.57 ppm), and toluene (2.36 ppm).

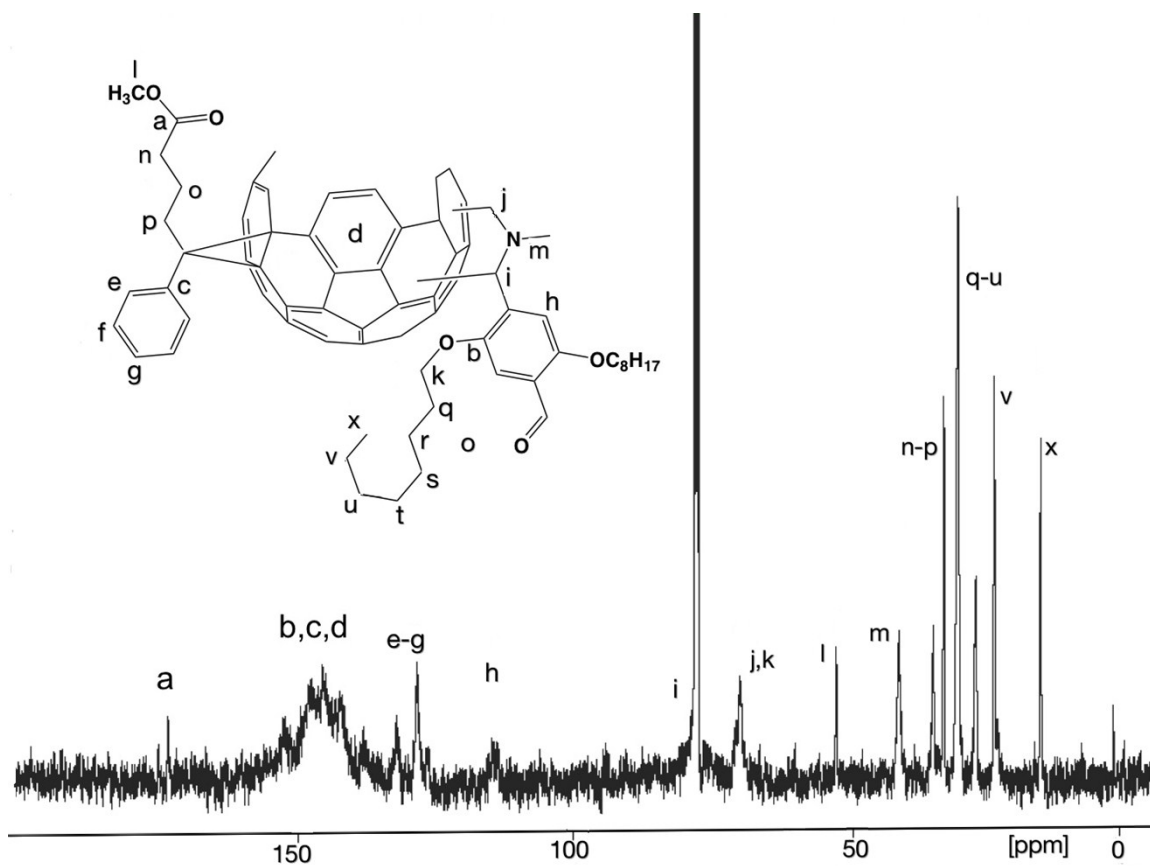


Figure S2. ^{13}C NMR (CDCl_3) of PPCBMB. Note peak due to grease (1.3 ppm).

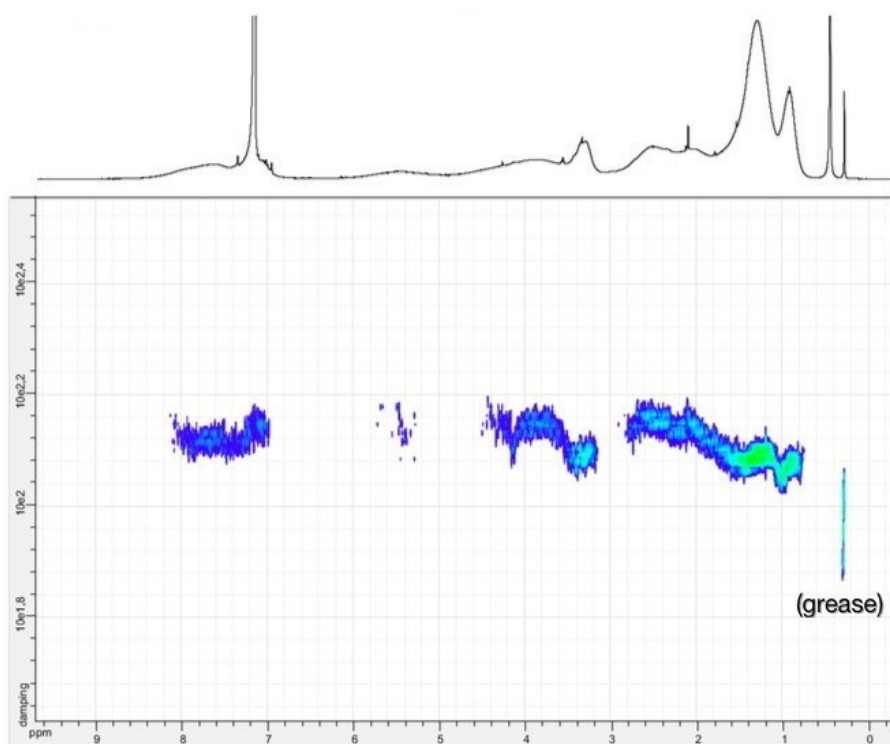


Figure S3. DOSY 2-D ^1H NMR (C_6D_6 , ambient temperature) of PPCBMB. Note the impurity due to grease at 0.1 ppm.

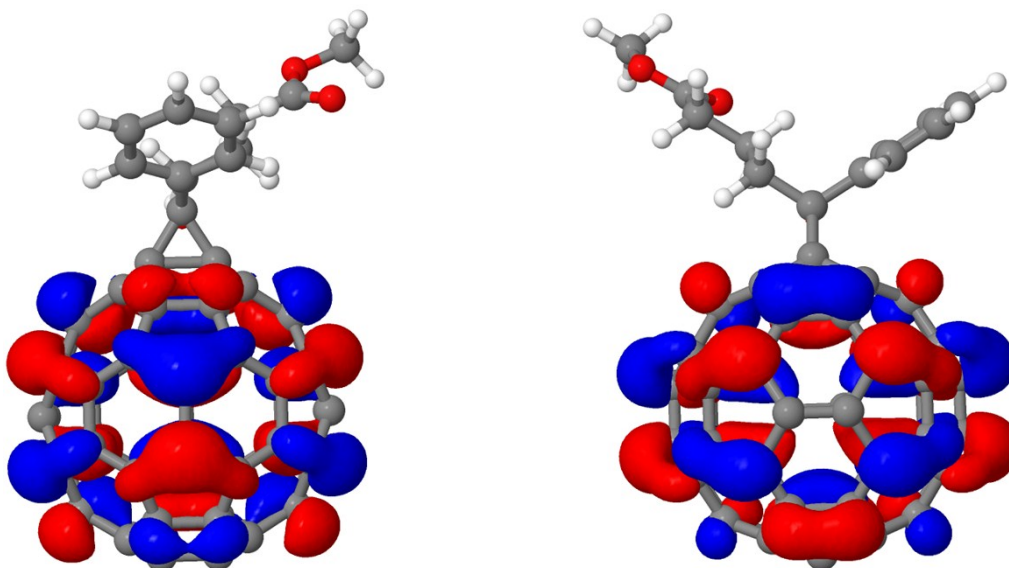


Figure S4. LUMO frontier orbitals for PCBM optimized using B3LYP/6-31G** level of theory. Note: The eight known attack positions for bis-adduct formation were studied by Time Dependent Density Functional Theory (TDDFT). The geometries were fully optimized within the B3LYP/6-31G** level of theory in the ground state. For all calculations the RIJCOSX approximation was used and run in Orca 3.0.2 software.^{S2,S5,S6}

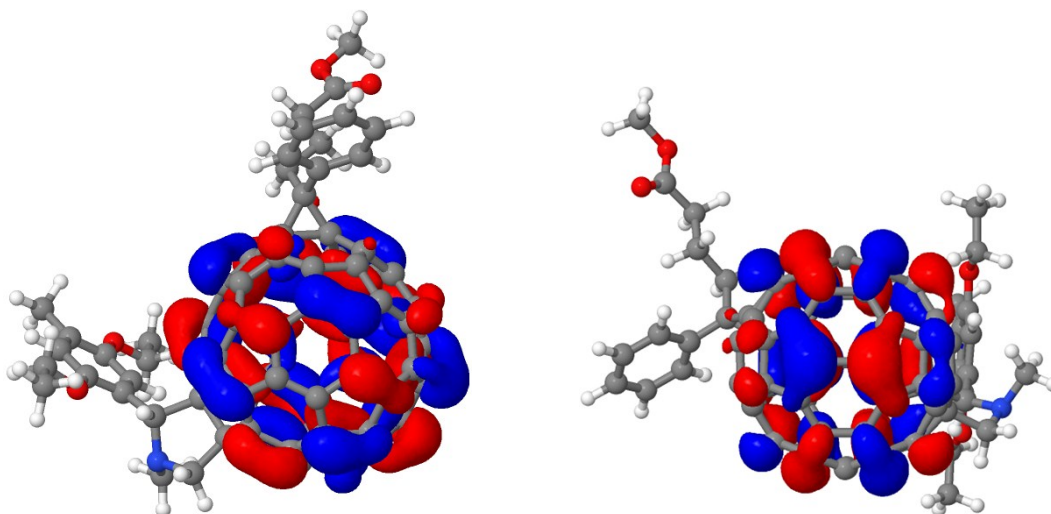


Figure S5. LUMO frontier orbitals for PCBM-1 optimized using B3LYP/6-31G** level of theory.

The vertical electron affinity (EA_v), adiabatic electron affinity (EA_{ad}), the chemical potential (μ), hardness (η), electrophilicity (ω), and the reorganization energies (λ) for subsequent gain and loss of an electron were similarly derived at the B3LYP/6-31G** level of theory using Orca 3.0.2 software and the results of the calculations are presented in Tables S1 and S2. The vertical electron affinity was calculated by removing one electron from the neutral molecule and not permitting geometrical relaxation, whereas for the adiabatic electron affinity, relaxation was allowed. The difference between the ground state total energy of the neutral molecule and the total energy of the reduced state gives the EA value. Within the vertical scenario, one can note that whichever attack happens to the fullerene sphere causes a decrease in the electron affinity.

The electrophilicity (ω) can be thought of as ‘electrophilic power’. It can be used to describe the resistance of the system to exchanging an electron with the surrounding environment, and is related to μ and η by:^{S7}

$$\omega = \frac{\mu^2}{2\eta}$$

In this case it was found that modifications reduced the electrophilicity, as expected, but also that the type of modification of the sphere and the presence of comonomer arms can impact negatively on ω .

Reorganization energies were calculated using an unrestricted open-shell wave function scheme for the Kohn-Sham orbitals. Although spin contamination is not systematic in DFT calculations, we monitored the mean value of $\langle S^2 \rangle$ in order to confine deviations within a maximum 10% of the expected value for a $\frac{1}{2}$ spin system. The ground state, however, was calculated in a restricted open-shell scheme, not allowing any spin polarization. It was found that the reorganization energies on electron transfer increase with successive modifications of the sphere, which may suggest a reduction in electron mobility at the molecular level.

	EA_v (eV)	EA_{ad} (eV)	μ (eV)	η (eV)	ω (eV)	LUMO (eV)
C₆₀	0	0	0	0	0	0
PCBM	-0.07	-0.06	0.24	-0.34	-0.08	0.13
PCBM-1	-0.23	-0.21	0.54	-0.61	-0.24	0.36
PCBM-2	-0.59	-0.55	0.88	-0.58	-0.53	0.80

Table S1. Energetic values calculated for C₆₀, PCBM, and the most probable structures PCBM-1 and PCBM-2.

	λ_1 (meV)	λ_2 (meV)	λ_T (meV)
C₆₀	0	0	0
PCBM	0.80	8.45	9.25
PCBM-1	6.98	25.96	32.93
PCBM-2	20.62	49.75	70.35

Table S2. Calculated reorganization energies (λ) with respect to the reference, C₆₀.

To sum, it should be noted that the values given in Tables S1 and S2 indicate general trends only at a molecular level; ^{S8,S9} morphological effects are not taken into account, and they may result in a reversal of the observed results.

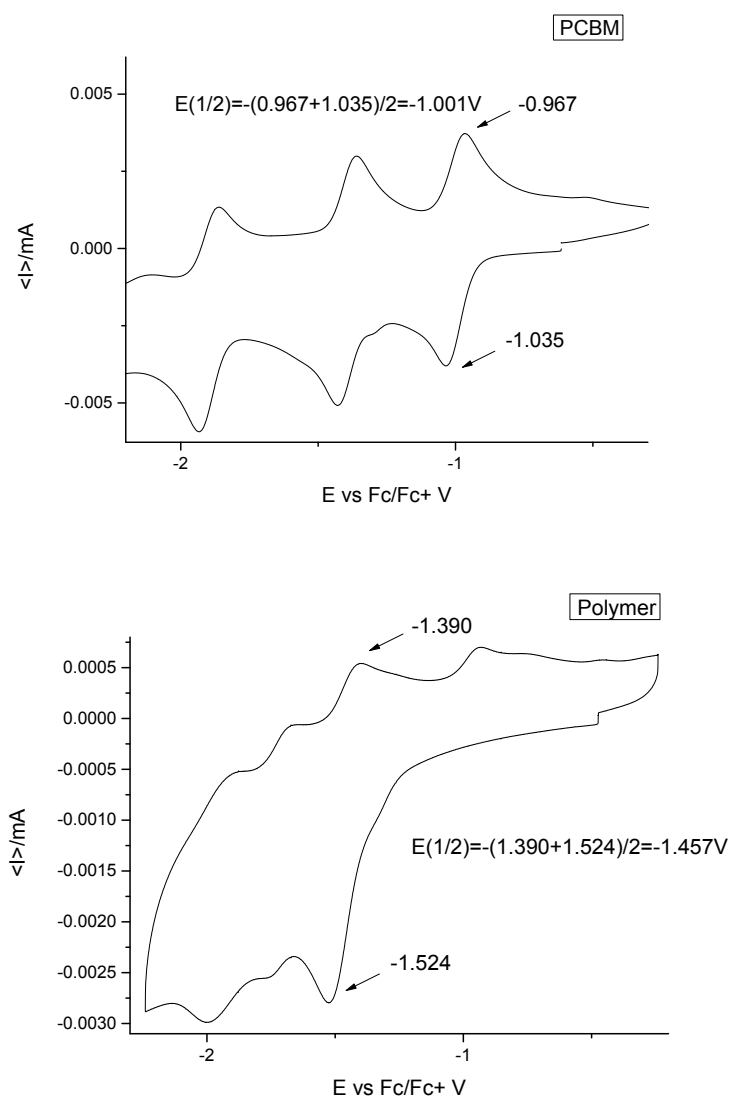


Figure S6. Cyclic voltammograms of: above, PCBM; and, below, PPCBMB.

Note: as detailed in the experimental above, the equation $E_{\text{LUMO}} = -(E_{1/2} + 4.8) \text{ eV}$ was used to give the values of $E_{\text{LUMO}}(\text{PCBM}) = -3.8 \text{ eV}$ and $E_{\text{LUMO}}(\text{PPCBMB}) = -3.34 \text{ eV}$. The value for PCBM found here compares well with that found in the literature, for example see reference S10.

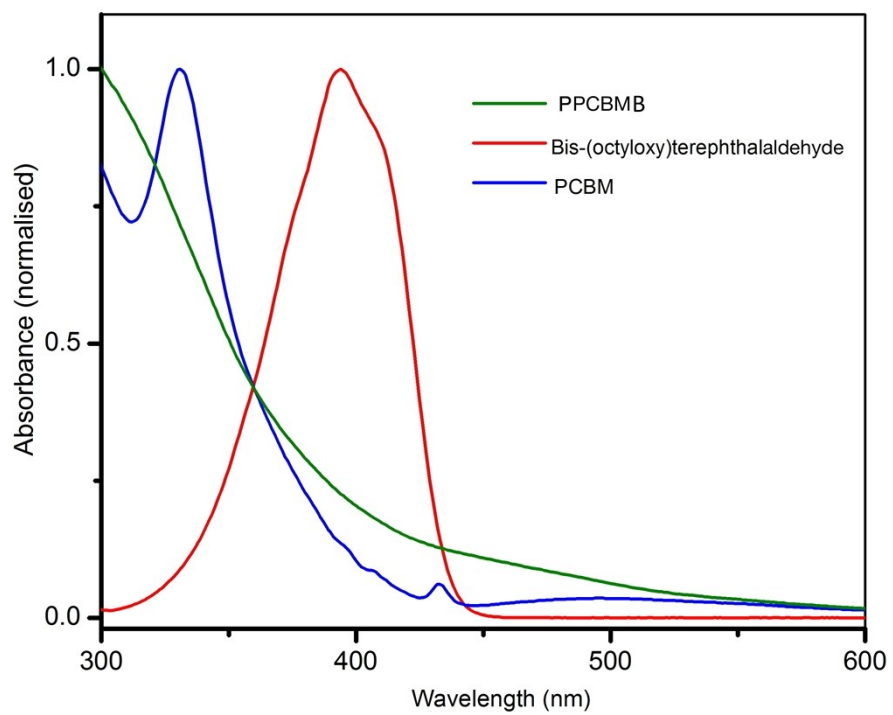


Figure S7. Normalized UV-visible absorption spectra (toluene) of: PCBM (blue), PPCBMB (green) and 2,5-bis(octyloxy)terephthalaldehyde (red).

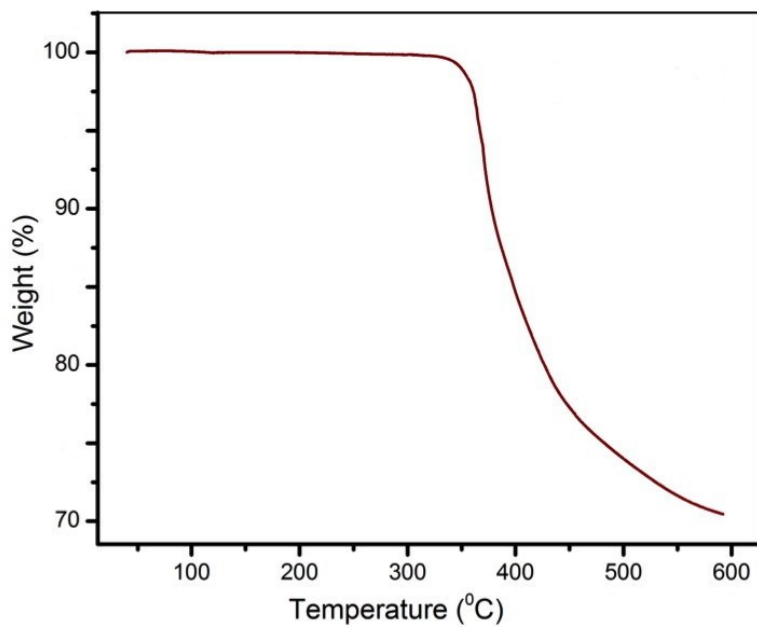


Figure S8. TGA of PPCBMB (N_2 , $10\text{ }^\circ\text{C min}^{-1}$).

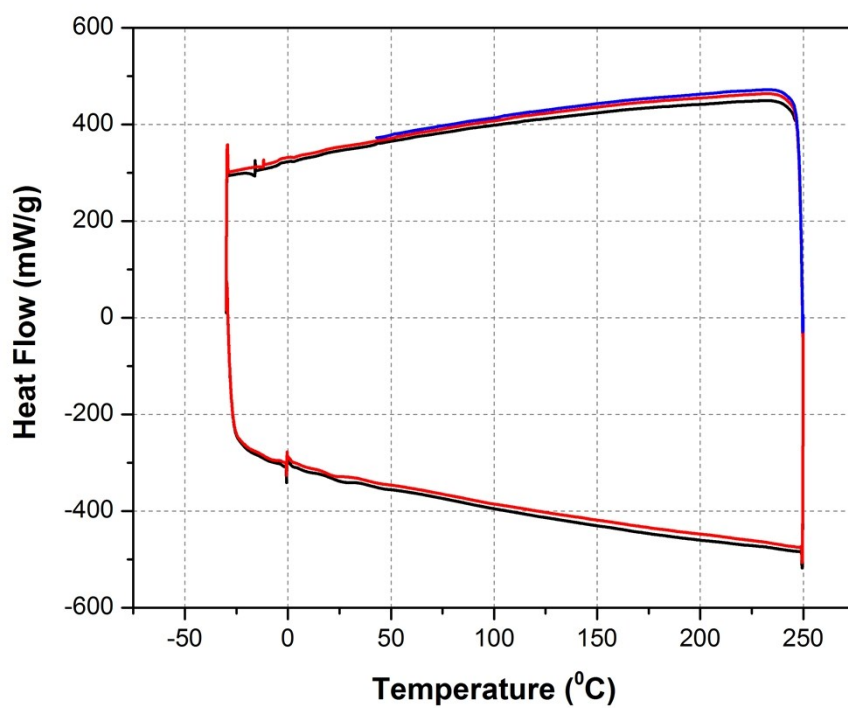


Figure S9. DSC thermogram of second and third heating cycles of PPCBMB ($10\text{ }^\circ\text{C min}^{-1}$).



Figure S10. Images of, above, PPCBMB, and below, a PPCBMB thin film (~50 nm) on ITO-glass substrate cast by blade coating from *o*-xylene.

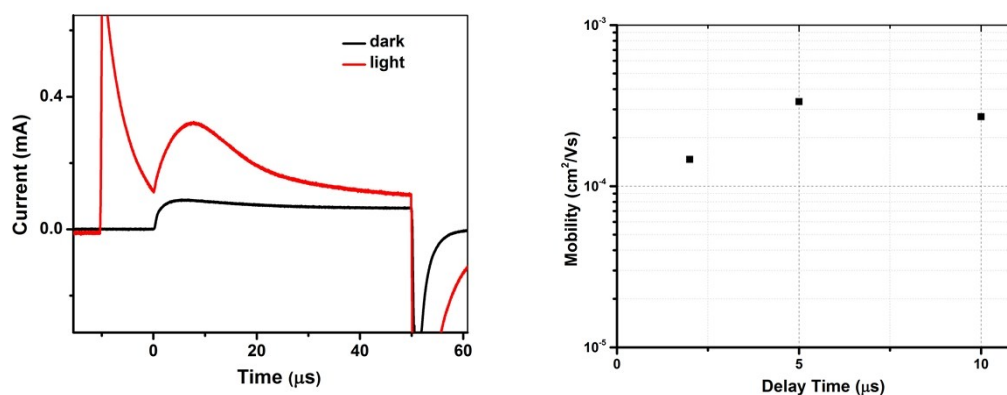


Figure S11. Photo-CELIV transients and corresponding mobility values for devices based on P3HT:PPCBMB active layer blends, at varying delay times between photo-generation and extraction.

References

- S1 J. Pommerehne, H. Vestweber, W. Guss, R. F. Mahrt, H. Bässler, M. Porsch and J. Daub, *Adv. Mater.* 1995, **7**, 551.
- S2 K. Kordatos, S. Bosi, T. Da Ros, A. Zambon, V. Luchini and M. J. Prato, *J. Org. Chem.* 2001, **66**, 2802.
- S3 F. Neese, *Wiley Interdisciplinary Reviews: Computational Molecular Science* 2012, **2**, 73.
- S4 a) G. Juška, K. Arlauskas, M. Viliūnas and J. Kočka, *Phys. Rev. Lett.* 2004, **84**, 4946; b) G. Juška, K. Arlauskas, M. Viliūnas, K. Genevičius, R. Österbacka and H. Stubb, *Phys. Rev. B* 2000, **62**, R16235.
- S5 F. Neese, F. Wennmohs, A. Hansen and U. Becker, *Chem. Phys.* 2009, **356**, 98.
- S6 T. Petrenko, S. Kossmann and F. Neese, *Chem. Phys.* 2011, **134**, 054116.
- S7 R. G. Parr, L. V. Szentpály and S. Liu, *J. Am. Chem. Soc.* 1999, **121**, 1922.
- S8 R. Stowasser and R. Hoffmann, *J. Am. Chem. Soc.* 1999, **121**, 3414.
- S9 E. J. Baerends and O. V. Gritsenko, *J. Phys. Chem. A* 1997, **101**, 5383.
- S10 S. Huang, F. Zhang, N. S. Knutson, M. T. Fontana, R. C. Huber, A. S. Ferreira, S. H. Tolbert, B. J. Schwartz and Y. Rubin, *J. Mater. Chem. A*. 2016, **4**, 416.